

Dynamics of entanglement in a two-mode nonlinear Jaynes-Cummings model

A. B. M. Ahmed^{1,a} and S. Sivakumar^{2,b}

¹Department of Physics, Indian Institute of Technology Madras
Chennai 600 036, India

²Materials Physics Division
Indira Gandhi Centre for Atomic Research Kalpakkam 603 102, India

^a abmahmed@physics.iitm.ac.in

^b siva@igcar.gov.in

November 9, 2018

Abstract

Dynamics of entanglement due to intensity-dependent interaction between a two-level atom and a single-mode electromagnetic field in a Kerr medium is studied. The form of the interaction is such that the Hamiltonian evolution is exactly solvable. The Hamiltonian is shown to be a deformed Jaynes-Cummings model admitting a closed, symmetric algebra. Dynamics of population inversion and atom-field entanglement are studied taking the initial state of the field to be either a coherent state or a squeezed vacuum. Analysis is extended to the case of a two-mode cavity field interacting with a two-level atom. For the two-mode case, the initial field is a pair coherent state or a two-mode squeezed vacuum. Effects due to nonlinearity, intensity-dependent interaction and detuning on the dynamics are discussed and compared with those of the single-mode case.

PACS: 42.50.Ct, 42.50.Dv, 03.67.Mn

I. Introduction

Quantum theory allows for correlations that are not possible in any classical stochastic process. The source of such correlations is entanglement [1]. Any system with two or more degrees of freedom has the possibility of being in an entangled state. Entangled states of atom and electromagnetic field in a cavity can be generated in the interaction of a two-level system with an external field. A well studied model of atom-field interaction is the Jaynes-Cummings (JC) model [2, 3, 4, 5], wherein the atom is treated as an electric-dipole interacting with a quantized electromagnetic field. The Hamiltonian is

$$\hat{H}_{JC} = \omega \hat{a}^\dagger \hat{a} + \frac{1}{2} \nu \hat{\sigma}_z + \lambda (\hat{a}^\dagger \hat{\sigma}_- + \hat{a} \hat{\sigma}_+), \quad (1)$$

where λ is the coupling constant, ω is the field frequency and ν is the atomic transition frequency. The operators \hat{a} and \hat{a}^\dagger are the annihilation and creation operators of the field; $\hat{\sigma}_z$ is the Pauli matrix, $\hat{\sigma}_+$ and $\hat{\sigma}_-$ are the raising and lowering operators of the atomic states. The ground and the excited states of the atom are represented by $|g\rangle$ and $|e\rangle$ respectively. The action of the relevant operators on these states are

$$\begin{aligned} \hat{\sigma}_z |e\rangle &= |e\rangle, \quad \hat{\sigma}_z |g\rangle = -|g\rangle, \\ \hat{\sigma}_+ |g\rangle &= |e\rangle, \quad \hat{\sigma}_+ |e\rangle = 0, \\ \hat{\sigma}_- |e\rangle &= |g\rangle, \quad \hat{\sigma}_- |g\rangle = 0. \end{aligned}$$

The first two terms in the Hamiltonian \hat{H}_{JC} correspond to the energies of the field and the atom respectively. The last term accounts for the atom-field interaction. This model has been used extensively in studying various quantum optical systems. A generalization of this model is useful in analysing position-dependent interaction strength [6, 7, 8]. To account for such a dependence, the interaction term is modified to

$$\hat{H}_{int} = \lambda (f(\hat{a}^\dagger \hat{a}) \hat{a} \hat{\sigma}_+ + \text{adjoint}). \quad (2)$$

The interaction term in the JC model is obtained when $f(\hat{a}^\dagger \hat{a}) = \hat{I}$, the identity operator. With any other form for $f(\hat{a}^\dagger \hat{a})$, the model is referred as Nonlinear Jaynes-Cummings(NJC) model. The operator-valued function f carries information about the position-dependent interaction strength. If the field has nonlinear dependence on the field amplitude, as in the case of Kerr interaction [9, 10, 11], the Hamiltonian is generalized further to

$$\hat{H} = \omega \hat{a}^\dagger \hat{a} + \frac{1}{2} \nu \hat{\sigma}_z + \chi \hat{a}^{\dagger 2} \hat{a}^2 + \lambda (f(\hat{a}^\dagger \hat{a}) \hat{a} \hat{\sigma}_+ + \text{adjoint}). \quad (3)$$

This Hamiltonian, with $f(\hat{a}^\dagger \hat{a}) = \hat{I}$, models the interaction between a field in a Kerr medium and a two-level atom. The quadratic term $\hat{a}^{\dagger 2} \hat{a}^2$ accounts

for the Kerr effect. We consider a special form of $f(\hat{a}^\dagger \hat{a})$, so chosen that the model Hamiltonian in Eq. (3) is exactly solvable [12, 13]. Choosing $f(\hat{a}^\dagger \hat{a}) = \sqrt{1 + k\hat{a}^\dagger \hat{a}}$, where $0 \leq k \leq 1$, the Hamiltonian \hat{H} is written as

$$\hat{H}_S = \omega \hat{K}^\dagger \hat{K} + \frac{1}{2} \nu \hat{\sigma}_z + \lambda (\hat{K}^\dagger \hat{\sigma}_- + \text{adjoint}), \quad (4)$$

where $\chi = k\omega$. The suffix ‘‘S’’ indicates that the Hamiltonian describes the interaction of a single-mode of a cavity field with a two-level atom. The operators $\hat{K} = \sqrt{1 + k\hat{a}^\dagger \hat{a}} \hat{a}$ and $\hat{K}^\dagger = \hat{a}^\dagger \sqrt{1 + k\hat{a}^\dagger \hat{a}}$ are deformed annihilation and creation operators respectively. In this work, the parameter k is taken to be nonnegative. Nevertheless, when $k = -1$, the operators \hat{K} and \hat{K}^\dagger are the well-known Holstein-Primakoff realization of spin operators. It is interesting to note that when $k = 0$, the Hamiltonian is the JC Hamiltonian. Nonzero values of k amount to including Kerr effect and intensity-dependent interactions. In essence, nonlinearity and intensity-dependent interactions are included *via* deformation. The operators \hat{K} , \hat{K}^\dagger and $\hat{K}_0 = k\hat{a}^\dagger \hat{a} + \frac{1}{2}$ satisfy the commutation relations,

$$[\hat{K}, \hat{K}^\dagger] = 2\hat{K}_0, \quad [\hat{K}_0, \hat{K}^\dagger] = k\hat{K}^\dagger, \quad [\hat{K}_0, \hat{K}] = -k\hat{K}, \quad (5)$$

with $[\ , \]$ denoting the commutator of the enclosed operators. Hence, the symmetric set $\{\hat{K}, \hat{K}^\dagger, \hat{K}_0\}$ forms a closed algebra under commutation. Further, when $k = 0$ the algebra is the Heisenberg-Weyl algebra generated by $\{\hat{a}, \hat{a}^\dagger, \hat{I}\}$. Another interesting limit corresponds to $k = 1$. In this case, the algebra defined in Eq. (5) is SU(1,1) algebra. Thus, two important algebras, namely, the Heisenberg-Weyl and the SU(1,1), are the special cases of the generalized algebra defined in Eq. (5). Mathematically, choosing nonzero k values amounts to deforming the Heisenberg-Weyl algebra. Thus, the Hamiltonian \hat{H}_S can be viewed as a deformed JC Hamiltonian. Though there is a formal resemblance between \hat{H}_{JC} and \hat{H}_S , the deformation ($k \neq 0$) allows to include nonlinearity and intensity-dependent coupling. Under suitable limits, the Hamiltonian \hat{H}_S approximates many well-studied Hamiltonians. For instance, when $k = 0$, \hat{H}_S becomes the usual JC model; when the mean photon number of the field satisfies $k\langle \hat{a}^\dagger \hat{a} \rangle \gg 1$, then $\sqrt{1 + k\hat{a}^\dagger \hat{a}} \sim \sqrt{k\hat{a}^\dagger \hat{a}}$ and \hat{H}_S approximates the Buck-Sukumar Hamiltonian [6].

In the single-mode field-atom bipartite system, the field is a continuous variable (infinite-dimensional Hilbert space) system while the atom is described in a two-dimensional Hilbert space. Recently, much work has been done on systems with two continuous variable subsystems; the entangled coherent states [14, 15] being the most widely studied. Such entangled continuous systems have desirable features which can be exploited in teleportation, quantum communication, etc [16, 14, 17, 18, 19, 20, 15, 21, 22]. Two-mode electromagnetic fields can be entangled by allowing them to interact with a two-level atom in a cavity. A basic scheme to perform this was

explored in [23] by employing a two-mode JC model. Various versions of the two-mode JC model [24] have been used in important contexts like the phase damping [25], entanglement distribution [26], entangling field modes with a moving atom [27], entropy squeezing [28] etc. In this work, a natural extension of \hat{H}_S is studied. One possibility is to consider

$$\hat{H}_T = \omega_1 \hat{K}_1^\dagger \hat{K}_1 + \omega_2 \hat{K}_2^\dagger \hat{K}_2 + \frac{1}{2} \hat{\sigma}_z + \lambda (\hat{K}_1^\dagger \hat{K}_2^\dagger \hat{\sigma}_- + \hat{K}_1 \hat{K}_2 \hat{\sigma}_+), \quad (6)$$

where $\hat{K}_1 = \sqrt{1 + k_1} \hat{a}^\dagger \hat{a}$ and $\hat{K}_2 = \sqrt{1 + k_2} \hat{b}^\dagger \hat{b}$. The creation operators of the two modes are \hat{a} and \hat{b} respectively; the corresponding annihilation operators are \hat{a}^\dagger and \hat{b}^\dagger . The suffix “T” indicates that the composite system involves a two-mode field. The operators \hat{K}_1 and \hat{K}_2 correspond to the two field modes of the cavity. The deformation parameters k_1 and k_2 satisfy $0 \leq k_1, k_2 \leq 1$. The operators in each of the sets $\{\hat{K}_1, \hat{K}_1^\dagger, \hat{K}_{10} = k_1 \hat{a}^\dagger \hat{a} + \frac{1}{2}\}$ and $\{\hat{K}_2, \hat{K}_2^\dagger, \hat{K}_{20} = k_2 \hat{b}^\dagger \hat{b} + \frac{1}{2}\}$, satisfy the closed algebra; defined in Eq. (5). The dynamics dictated by the two-mode Hamiltonian \hat{H}_T is exactly solvable. This Hamiltonian, like its one-mode counterpart \hat{H}_S , approximates, many of the known two-mode JC models. For instance, if $k_1 = k_2 = 0$ then \hat{H}_T corresponds to the Hamiltonian studied in the context of phase damping [25]. When the mean photon number is large enough so that $1 + k \langle \hat{a}^\dagger \hat{a} \rangle \approx k \langle \hat{a}^\dagger \hat{a} \rangle$ and $1 + k \langle \hat{b}^\dagger \hat{b} \rangle \approx k \langle \hat{b}^\dagger \hat{b} \rangle$, then the interaction term is approximated by $\sqrt{\hat{b}^\dagger \hat{b}} \sqrt{\hat{a}^\dagger \hat{a}} \hat{a} \hat{b} \hat{\sigma}_+ + \text{adjoint}$ and the resulting Hamiltonian is the two-mode Buck-Sukumar Hamiltonian.

In the present work, dynamics dictated by the Hamiltonian \hat{H}_S and \hat{H}_T are studied; in particular, the dynamics of population inversion and of entanglement are analyzed. This paper is organized in the following way. Results on the single-mode system are presented first and those on the two-mode system are presented subsequently. In section II, dynamics of entanglement in the single mode case is discussed. The effects of nonlinearity and intensity-dependent coupling on the dynamics are studied. In section III, analyses on two-mode case are presented. Dynamics of various tangles in the system are studied, and wherever possible, the results are compared with those of the single mode case.

II. Single-mode NJC model

In the single-mode NJC model, there are two degrees of freedom in the system, corresponding to the field and the two-level atom respectively. The Hamiltonian of the system is taken to be \hat{H}_S . The initial state of the atom-field system is taken to be a product state. Entanglement between the atom and the field is generated by the interaction. The time evolution of the

atom-field state is obtained by solving

$$i\frac{\partial}{\partial t}|\psi(t)\rangle = \hat{H}_S|\psi(t)\rangle, \quad (7)$$

where $|\psi(t)\rangle$ represents the state of the atom-field system at time 't'. The explicit form of $|\psi(t)\rangle$ is $\sum_{n=0}^{\infty} [C_{e,n}(t)|e, n\rangle + C_{g,n}(t)|g, n\rangle]$; the state $|e, n\rangle$ [respectively, $|g, n\rangle$] represents the field in the number state $|n\rangle$ and the atom in the state $|e\rangle$ [respectively, $|g\rangle$]. The coefficients $C_{e,n}(t)$ and $C_{g,n}(t)$ are [13]

$$e^{-i\Delta_n t/2} C_{e,n}(t) = [\cos(\frac{\Omega_n t}{2}) - \frac{i\Delta_n}{\Omega_n} \sin(\frac{\Omega_n t}{2})] C_{e,n}(0) - \frac{2i\lambda\eta_n}{\Omega_n} \sin(\frac{\Omega_n t}{2}) C_{g,n+1}(0), \quad (8)$$

$$e^{i\Delta_n t/2} C_{g,n+1}(t) = [\cos(\frac{\Omega_n t}{2}) + \frac{i\Delta_n}{\Omega_n} \sin(\frac{\Omega_n t}{2})] C_{g,n+1}(0) - \frac{2i\lambda\eta_n}{\Omega_n} \sin(\frac{\Omega_n t}{2}) C_{e,n}(0), \quad (9)$$

where $\Delta = \nu - \omega$, $\Delta_n = \Delta - 2k\omega n$, $\Omega_n = \sqrt{\Delta_n^2 + 4\lambda^2\eta_n^2}$ and $\eta_n = \sqrt{(1+n)(1+kn)}$. These analytical results have been used to arrive at the results presented subsequently.

The initial state of the field is taken to be either a coherent state,

$$|\alpha\rangle = e^{-\frac{|\alpha|^2}{2}} \sum_{n=0}^{\infty} \frac{\alpha^n}{\sqrt{n!}} |n\rangle, \quad \alpha \in C, \quad (10)$$

or a squeezed vacuum

$$|z\rangle = \frac{1}{\sqrt{\cosh r}} \sum_{l=0}^{\infty} (-1)^l \frac{\sqrt{(2l)!}}{2^l l!} (e^{i\theta} \tanh r)^l |2l\rangle, \quad z = re^{i\theta}, \quad r = |z|. \quad (11)$$

The states considered in this work correspond to $\alpha = \sqrt{30}$ and $z = 2.402$. The values are chosen so that the mean number of photons in the CS and that in the SV are equal to 30. The initial state of the system is $(\sum_n f_n |e, n\rangle)$, where the coefficients f_n of the field state are chosen to be those of $|\alpha\rangle$ or $|z\rangle$. Thus, the initial conditions, $C_{e,n}(0)$ and $C_{g,n}(0)$, are

$$C_{e,n}(0) = f_n; \quad C_{g,n}(0) = 0. \quad (12)$$

These are the initial conditions when the atom evolves from its excited state. The density operator for the system is the projection operator $|\psi(t)\rangle\langle\psi(t)|$, expressed in the $\{|e, n\rangle, |g, n\rangle\}$ basis as

$$\hat{\rho} = |\psi(t)\rangle\langle\psi(t)| = \sum_{a,b=e,g} \sum_{n,m=0}^{\infty} C_{a,n}(t) C_{b,m}^*(t) |a, n\rangle\langle b, m|. \quad (13)$$

Population inversion $W_S(t)$ is defined as the difference in the probabilities of the atom to be in the states $|e\rangle$ and $|g\rangle$. Hence,

$$W_S(t) = \text{Tr}[\hat{\rho}\hat{\sigma}_z] = \sum_{n=0}^{\infty} [|C_{e,n}(t)|^2 - |C_{g,n}(t)|^2], \quad (14)$$

where Tr stands for tracing over both the atomic and field states. Evolution of $W_S(t)$ is shown in Fig. 1, when the field is initially the coherent state $|\alpha\rangle$. The figures stacked in the first column correspond to $k = 0$; the second and third columns correspond to $k = 10^{-4}$ and $k = 10^{-3}$ respectively. Different rows of figures give information on the effect of detuning. The figures in the first row correspond to $\Delta = 0$. A special feature of the Hamiltonian \hat{H}_S is the existence of a minimum for the Rabi frequency Ω_n , for some $n = \bar{n}$. The numerical value of \bar{n} is related to the other parameters through [13]

$$\bar{n} = \frac{k\Delta - \lambda^2\omega^2(1+k)}{2k\omega(k + \lambda^2)}. \quad (15)$$

If the mean value of $\langle \hat{a}^\dagger \hat{a} \rangle$ is chosen to be \bar{n} , the corresponding Δ satisfying the Eq. (15) is the critical detuning Δ_c . In the resonant JC model ($k = 0, \Delta = 0$), the perfect collapses of the population inversion are Gaussian modulated cosines [29, 30]. The dynamics of $W_S(t)$ is known to have distinct features, such as ‘super structures’ in the ‘collapse - revival’ pattern, when $\Delta \approx \Delta_c$, *i.e.*, the envelope of collapse or revival is not a Gaussian modulated cosine [9]. This is shown in the figure located at the third row of the second column in Fig. 1. It is to be noted that a minimum in the Rabi frequency is possible only when $k \neq 0$.

The first column of figures in Fig. 1 shows the effect of higher detuning on the dynamics of $W_S(t)$. Larger detuning inhibits the interaction between the atom and the field. This is expected based on the Fermi’s Golden rule which states that interaction probability becomes smaller as the field frequency deviates from the resonant condition. Hence, with large detuning the atom evolves such that it has substantial overlap with its initial state. The last figure corresponds to $\Delta = 0.016$ and the $W_S(t)$ profile indicates that the atom practically remains in the excited state.

Dynamics dictated by \hat{H}_S differs from that of \hat{H}_{JC} due to the Kerr term and the intensity-dependent interaction in \hat{H}_S . The strength of the nonlinearity ($\propto k\hat{a}^{\dagger 2}\hat{a}^2$) and that of the coupling ($\propto \sqrt{1+k}\hat{a}^\dagger\hat{a}$) increase with k . It is found that if $k = 0.01$, even under resonant condition, the state of the atom has substantial overlap with the excited state $|e\rangle$. This implies that the presence of cavity field has not resulted in any significant change of atomic state. As noted earlier, the atom-field interaction becomes insignificant if the interaction is non-resonant due to large detuning in the usual JC

model, which is the undeformed \hat{H}_S . Thus, the effect of large “ k ” mimics the effect of large detuning. The origin of this “inhibition of emission” from the excited state is mostly due to the nonlinear term $k\hat{a}^\dagger{}^2\hat{a}^2$. In the case of coherent states, $k\hat{a}^\dagger{}^2\hat{a}^2$ term contributes $|\alpha|^4 + |\alpha|^2$ to the total energy while the contribution from the interaction term $\sqrt{1 + k\hat{a}^\dagger\hat{a}}\hat{a}$ is $\sim \sqrt{1 + k}|\alpha|^2\alpha$. For small value of mean photon number ($\langle\hat{a}^\dagger\hat{a}\rangle \sim 1$), the contributions of the nonlinear term and the interaction term to the energy are nearly equal. However, for large amplitude coherent state, the nonlinear term dominates over the interaction. To bring out these features the variation of $W_S(t)$ is plotted in Fig. 3 for $|\alpha|^2 = 1$ and $|\alpha|^2 = 30$. The interaction is assumed to be resonant. From the figures it is seen that as k increases, the quantity $W_S(t)$ stays close to unity if $|\alpha|^2 = 30$ and oscillates if $|\alpha|^2 = 1$. In the large amplitude case, the population inversion remains close to unity while it swings between 1 and 0.2 when $|\alpha|^2 \sim 1$. The former corresponds to dominant nonlinearity while the later corresponds to nearly equal magnitudes of the nonlinearity and the interaction. Thus, the “inhibition of emission”, despite the presence of a resonant field, is due to the nonlinear term.

Even at smaller values of k the effect of nonlinearity can be dominant. The last column of Fig. 1 corresponds to $k = 10^{-3}$, an order of magnitude smaller than 10^{-2} . The initially excited atom is left almost undisturbed in the resonant case as evident from the nearly time-independent $W_S(t)$. As the detuning increases, the atom begins to interact with the field, and, consequently, the oscillations in $W_S(t)$ are larger. This is inferred by comparing the figures in the first row (zero detuning) of Fig. 1 with those in the successive rows (higher detunings). These counter-intuitive features, that is, noninteracting, resonant field and interacting, non-resonant field, are due to the presence of nonlinearity.

In Fig. 2, the dynamics of $W_S(t)$ is shown when the field is initially a squeezed vacuum. Some of the features present in the interaction of the atom with coherent state are absent. Even though, the mean number of photons in the squeezed vacuum is chosen to satisfy Eq. (15), there are no “super” structures in the population inversion. However, as in the coherent state case, the field-atom interaction is strengthened at nonzero detuning when the value of the deforming parameter k is nonzero but small (10^{-3}). The mean number of photons in the CS and the SV are the same. Hence, the differences in the dynamics are due to the different photon statistics of the two states.

Interaction between the atom and the field entangles them. The initial state $\sum f_n|e, n\rangle$ is a product state and hence the entanglement is zero. To study the effectiveness of the interaction in entangling the atom and field system, linear entropy is used as the measure of entanglement. If $\hat{\rho}$ is the density operator of the composite system, its linear entropy (L) is defined as

$$L = 2(1 - \text{Tr}[\hat{\rho}_f^2]) = 2(1 - \text{Tr}[\hat{\rho}_a^2]). \quad (16)$$

Here $\hat{\rho}_f$ [respectively, $\hat{\rho}_a$] is the reduced density operator of the field [respectively, atom] obtained by partially tracing over the atomic [respectively, field] states. For instance, the reduced density operator $\hat{\rho}_a$ for the atom is

$$\hat{\rho}_a = \begin{pmatrix} \sum_n |C_{e,n}(t)|^2 & \sum_n C_{e,n}^*(t) C_{g,n}(t) \\ \sum_n C_{e,n}(t) C_{g,n}^*(t) & \sum_n |C_{g,n}(t)|^2 \end{pmatrix}. \quad (17)$$

Even though other measures such as von Neumann entropy exist, in the case of pure states all entanglement measures are equivalent. In this work, linear entropy is used as the entanglement measure as it is easier to compute. The two quantities, namely, W_S and L , are related by

$$L = 1 - W_S^2 - 4|\sum C_{e,n}^* C_{g,n}|^2. \quad (18)$$

The quantity $|\sum C_{e,n}^* C_{g,n}|$ is the atomic coherence since this particular term appears as off-diagonal element in the reduced density matrix of the atom. The time-evolution of population inversion shows a striking resemblance to the entanglement if the initial field state is a squeezed vacuum, see Figs. 2 and 5. This feature is not to be seen in the case of coherent states, see Figs. 1 and 4. This observation is explained by the relationship, Eqn. (18), between the linear entropy and the population inversion. It turns out, as indicated by numerical calculations, that the atomic coherence vanishes during evolution if the initial state is a squeezed vacuum. Consequently, $L = 1 - W_S^2$ and there is a good resemblance of the $L(t)$ and $W_S(t)$ profiles. In the case of CS, the atomic coherence is not small. As a result, the $L(t)$ and $W_S(t)$ profiles do not match. Interestingly, in this case the atomic coherence spikes to larger values during the course of evolution. Whenever, the coherence is large, the reduced density matrix is less mixed. This, in turn, means that the entanglement of the composite system is less. This is the origin of low entanglement spikes in the case of atom-coherent state interaction, refer Fig. 4.

The time-evolution of linear entropy (L) is shown in Fig. 4, when the cavity field is initially a coherent state. In Fig. 5, results on the dynamics of L are given for the squeezed vacuum case. The first row of the figures correspond to $\Delta = 0$ (resonant case). The figures in the first column correspond to $k = 0$ while those in the second column correspond to $k = 10^{-3}$. In the resonant case, the amplitude of variation of L smaller if the value of k is nonzero. The effect of deformation is to minimize the effectiveness of the interaction in entangling the atom and the resonant field. This readily corroborates with the fact that the population inversion is nearly unity for this case, refer Fig. 1 and 2. Higher values of population inversion (≈ 1) imply that the atomic state is $\approx |e\rangle$; consequently, the composite system is a product state and the linear entropy (equivalently, the entanglement) is nearly zero. Hence, with the increase of k , the entanglement in the atom-field system becomes zero, even in the resonant case. In the non-resonant NJC model, higher values of k make the time-evolved atomic state to have substantial overlap with the ground state. This is in contrast with the non-resonant JC model in which the interaction becomes less effective in causing

Table 1: Mean entanglement in single-mode NJC model

Δ	k	Mean entanglement	
		Coherent state	Squeezed vacuum
0	0	0.84	0.97
0	1×10^{-4}	0.89	0.94
0	1×10^{-3}	0.04	0.34
0.01	0	0.56	0.64
0.01	1×10^{-4}	0.91	0.77
0.01	1×10^{-3}	0.75	0.26
0.0161	0	0.3	0.44
0.0161	1×10^{-4}	0.74	0.62
0.0161	1×10^{-3}	0.81	0.24

transitions as detuning increases. Thus, in the non-resonant case, the NJC interaction is more effective in entangling the atom and the field than the JC interaction.

A simpler way of assessing the effectiveness of the interaction in entangling the field and the atom is to study the mean entanglement \bar{L} , defined as [31]

$$\bar{L} = \frac{1}{T} \int_0^T L(t') dt', \quad (19)$$

is used. The value of T is chosen so that gT is 100. The values of the mean entanglement is shown in Table 1 for the single mode case. Small nonzero values of k , of the order of 10^{-4} leads to better entanglement than zero or large values for k . In the resonant case \bar{L} approaches zero as k increases from 10^{-4} to 10^{-3} . In the non-resonant case the entanglement does not become small even if k increases to 10^{-3} . It is interesting to note that in the single-mode case, entanglement is more effective in the non-resonant case if the initial field is a CS in comparison to the case of initial field being in the SV.

III. Two mode NJC model

In this section, the interaction between a two-level atom and a two-mode cavity field is studied. Two types of fields are considered: pair coherent (PC) state $|\zeta\rangle$ [32] and two-mode squeezed vacuum $|\mu\rangle$ (TSV) [33]. The respective Fock state representations are:

$$|\zeta\rangle = N_0 \sum_n \frac{\zeta^n}{n!} |n, n\rangle, \quad (20)$$

where $N_0 = 1/\sqrt{I_0(2|\zeta|)}$, $I_0(2|\zeta|)$ is the modified Bessel function of order

zero and $\zeta \in C$ is the amplitude of the state;

$$|\mu\rangle = \sqrt{1 - |\mu|^2} \sum_n \mu^n |n, n\rangle, \quad (21)$$

where $\mu \in C$ is the amplitude of state and $0 \leq |\mu| < 1$. Both these states involve superposition of paired states $|n, n\rangle$, which have equal number of quanta in both modes. The unpaired states $|n, m\rangle (n \neq m)$ are not present. In the quantum entanglement context, the TSV is an important example of entangled Gaussian state and the PC state is entangled but non-Gaussian. Interestingly, TSV arises also in the context of teleportation of uniformly accelerated objects[34].

The Hamiltonian of the system is taken to be \hat{H}_T , the two-mode extension of \hat{H}_S . The state of the system at time “t” is $|\Psi(t)\rangle = \sum_{n=0}^{\infty} (C_{e,n,n}(t)|e, n, n\rangle + C_{g,n,n}(t)|g, n, n\rangle)$. Unpaired states are absent in the evolved state $|\Psi(t)\rangle$ as well. This feature is due to the type of interaction being considered and the absence of unpaired states in the initial state. In what follows, we set $k_1 = k_2 = k$. With this choice for the two deformation parameters, the interaction term $\hat{H}_I = \lambda\sqrt{(1 + k\hat{a}^\dagger\hat{a})(1 + k\hat{b}^\dagger\hat{b})}\hat{a}\hat{b}\hat{\sigma}_+ + \text{adjoint}$ gives,

$$\hat{H}_I|e, n, n\rangle = \lambda(1 + kn + k)|g, n + 1, n + 1\rangle, \quad (22)$$

$$\hat{H}_I|g, n, n\rangle = \lambda(1 + kn - k)|e, n - 1, n - 1\rangle. \quad (23)$$

That is, a paired state is transformed to another paired state. More precisely, under the action of \hat{H}_T , the paired state $|e, n, n\rangle$ becomes the paired state $|g, n + 1, n + 1\rangle$ and vice-versa. Hence, the evolved state is a superposition of paired states if the initial state is a superposition of paired states. Another consequence is that there are invariant subspaces in the Hilbert space of the tripartite system. It is easily recognized from the transformations indicated in Eqs. (21) and (22), that the span of $\{|e, n, n\rangle, |g, n + 1, n + 1\rangle\}$, for a fixed n , is invariant under the action of \hat{H}_I . Moreover, the invariant subspaces are disjoint. These features imply that the dynamics of the coefficients $C_{e,n,n}(t)$ and $C_{g,n+1,n+1}(t)$ are coupled to each other and do not depend on the dynamics of other coefficients. The Schrodinger equation for the dynamics of the coefficients $C_{e,n,n}(t)$ and $C_{g,n+1,n+1}(t)$ is the matrix equation,

$$i\frac{d}{dt} \begin{pmatrix} C_{e,n,n}(t) \\ C_{g,n+1,n+1}(t) \end{pmatrix} = \begin{bmatrix} h_{11} & h_{12} \\ h_{21} & h_{22} \end{bmatrix} \begin{pmatrix} C_{e,n,n}(t) \\ C_{g,n+1,n+1}(t) \end{pmatrix}. \quad (24)$$

Here $h_{11} = \omega_1(n + \frac{1}{2} + kn^2 - kn) + \omega_2(n + \frac{1}{2} + kn^2 - kn) + \frac{\Delta}{2}$, $h_{22} = \omega_1(n + \frac{1}{2} + kn^2 + kn) + \omega_2(n + \frac{1}{2} + kn^2 + kn) - \frac{\Delta}{2}$, and $h_{12} = h_{21} = \lambda(1 + n)(1 + kn)$. Here, $\Delta = \nu - (\omega_1 + \omega_2)$ is the detuning. This matrix equation is solved to give

$$e^{-i\Delta_{n,n}t/2}C_{e,n,n}(t) = [\cos(\frac{\Omega_{n,n}t}{2}) - \frac{i\Delta_{n,n}}{\Omega_{n,n}}\sin(\frac{\Omega_{n,n}t}{2})]C_{e,n,n}(0)$$

$$-\frac{2i\lambda\eta_{n,n}}{\Omega_{n,n}} \sin\left(\frac{\Omega_{n,n}t}{2}\right) C_{g,n+1,n+1}(0), \quad (25)$$

$$\begin{aligned} e^{i\Delta_{n,n}t/2} C_{g,n+1,n+1}(t) &= \left[\cos\left(\frac{\Omega_{n,n}t}{2}\right) + \frac{i\Delta_{n,n}}{\Omega_{n,n}} \sin\left(\frac{\Omega_{n,n}t}{2}\right) \right] C_{g,n+1,n+1}(0) \\ &\quad - \frac{2i\lambda\eta_{n,n}}{\Omega_{n,n}} \sin\left(\frac{\Omega_{n,n}t}{2}\right) C_{e,n,n}(0), \end{aligned} \quad (26)$$

where $\Delta_{n,n} = \Delta - 2k\omega_1n - 2k\omega_2n$, $\Omega_{n,n} = \sqrt{\Delta_{n,n}^2 + 4\lambda^2\eta_{n,n}^2}$ and $\eta_{n,n} = (1+n)(1+kn)$. These analytical solutions are used in calculating population inversion and entanglement measures in the tripartite system.

The reduced density operator $\hat{\rho}_A$ for the atomic system is

$$\hat{\rho}_A = \begin{pmatrix} \sum_n |C_{e,n,n}(t)|^2 & \sum_n C_{e,n,n}^*(t) C_{g,n,n}(t) \\ \sum_n C_{e,n,n}(t) C_{g,n,n}^*(t) & \sum_n |C_{g,n,n}(t)|^2 \end{pmatrix}. \quad (27)$$

For the two-mode case, the population inversion, denoted by $W_T(t)$, is given by

$$W_T(t) = \sum_n [|C_{e,n,n}(t)|^2 - |C_{g,n,n}(t)|^2]. \quad (28)$$

The evolution of population inversion is given in Fig. 6 for the PC state and in Fig. 7 for the TSV. In both the figures, the successive columns correspond to $k = 0$ and $k = 2 \times 10^{-3}$ respectively. And the successive rows correspond to different detuning parameter values (Δ) starting from zero detuning. In the resonant two-mode JC model, *i.e.*, $\Delta = 0$ and $k = 0$, the Rabi frequencies satisfy $\Omega_{n,n}t = gt(1+n)$; these frequencies are commensurate and so the dynamics is periodic. As a consequence, $W_T(t)$ shows periodic features in the resonant two-photon JC model. At the time instances when $gt = l\pi$ (l , a positive integer) the atom returns to the initial state, unlike in the single mode case. This periodicity is destroyed in the non-resonant interaction as the Rabi frequencies are incommensurate. The atomic evolution from the excited state is increasingly inhibited with larger detuning which is evident from the column 1 of Figs. 6 and 7. It is to be noted that the Rabi frequency $\Omega_{n,n}$ depends only on a single quantum number “ n ”, a consequence of the initial field being a superposition of paired state. As a function of n , the two-mode Rabi frequency exhibits a minimum at $n = \bar{n}$, obtained by solving $\frac{\partial \Omega_{n,n}}{\partial t}|_{n=\bar{n}} = 0$, provided $k \neq 0$. The detuning corresponding to $n = \bar{n}$ is called critical detuning, which is given as

$$\Delta_{\bar{n},\bar{n}} = \Delta'_c = k\omega\bar{N} + \frac{g^2}{k\omega}[(1+k)(2+\bar{N}+k\bar{N} + \frac{3}{2}\bar{N}^2k) + \frac{1}{2}\bar{N}^3k^2], \quad (29)$$

where $\bar{N} = 2\bar{n}$ is the total mean photon number of the two-mode radiation field. At critical detuning, the evolution of $W_T(t)$ has noticeable features.

The envelope of $W_T(t)$ appears periodic and this is lost when detuning shifts away from Δ'_c . This is seen by comparing the figures in the third row ($\Delta = \Delta'_c$) with the those in the second row ($\Delta < \Delta'_c$) of Fig. 6. Further, nonzero k value (refer the second column of Fig. 6) significantly influences the envelope pattern in the population inversion. As in the case of single mode NJC, the critical detuning alters the population inversion dynamics qualitatively. A difference in the evolution at critical detuning, in the single-mode and two-mode cases is to be pointed out. In the single-mode case, super structures are seen if the initial field state is a CS while such structures are not prominent if the initial state is a SV. But in the two-mode case, similar structures in the envelope of $W_T(t)$ are observed whether the initial field state is a PC state or a TSV.

The system described by \hat{H}_T is a tripartite system: a two-level atom and two field modes. The Hilbert spaces associated with the field modes are of infinite dimension. There is no known measure of entanglement if any subsystem of a tripartite system is of infinite dimension. An assessment of entanglement in the system is obtained by studying bipartite entanglement in different partitions of the system. In the present case, the relevant partitions are: (i) two-level atom as a subsystem and the two field modes together form the other subsystem; (ii) two-level atom along with one of the field modes as one subsystem and the other field mode as the other subsystem; and (iii) the third possibility is to exchange the roles of the fields in the previous case. The entanglement measures of the different bipartite partitions are called tangles (T). The states considered in this work are pure states and hence the various tangles are chosen to be the respective von Neumann or linear entropies. Thus,

$$T_{A,F_1 \otimes F_2} = 2[1 - \text{Tr}(\hat{\rho}_A^2)] = 2[1 - \text{Tr}(\hat{\rho}_{F_1 \otimes F_2}^2)], \quad (30)$$

$$T_{A \otimes F_1, F_2} = -\text{Tr}[\hat{\rho}_{A \otimes F_1} \log_2(\hat{\rho}_{A \otimes F_1})] = -\text{Tr}[\hat{\rho}_{F_2} \log_2(\hat{\rho}_{F_2})], \quad (31)$$

$$T_{A \otimes F_2, F_1} = -\text{Tr}[\hat{\rho}_{A \otimes F_2} \log_2(\hat{\rho}_{A \otimes F_2})] = -\text{Tr}[\hat{\rho}_{F_1} \log_2(\hat{\rho}_{F_1})]. \quad (32)$$

The suffix $(A, F_1 \otimes F_2)$ indicates that the atom is treated as a subsystem and the two field modes (F_1 and F_2) are treated as a single entity is another subsystem of the relevant partition. Similar convention is adapted for the other suffixes. The initial field state, a superposition of paired states is symmetric under the exchange of photon numbers of the two modes and this symmetry is preserved during evolution. Consequently, $T_{A \otimes F_1, F_2}$ and $T_{A \otimes F_2, F_1}$ are identical. In Figs. 8 and 9, only $T_{A \otimes F_1, F_2}$ is shown. The calculation of $T_{A \otimes F_1, F_2}$ requires the reduced density matrix of the atom and the first mode, which is

$$\begin{aligned} \hat{\rho}_{A \otimes F_1} &= \sum_n |C_{e,n,n}|^2 |en\rangle\langle en| + C_{e,n,n} C_{g,n,n}^* |en\rangle\langle gn| \\ &\quad + C_{g,n,n} C_{e,n,n}^* |gn\rangle\langle en| + |C_{g,n,n}|^2 |gn\rangle\langle gn|. \end{aligned} \quad (33)$$

Another quantity that is of interest is the entanglement between the two field modes. Quantum relative entropy E_{F_1, F_2} is a measure of entanglement

in a bipartite field state involving only the paired states [35]. The field density matrix is

$$\hat{\rho}_{F_1, F_2} = \sum_{r=e, g} \langle r | \Psi(t) \rangle \langle \Psi(t) | r \rangle \quad (34)$$

$$= \sum_{n, m} a_{n, m} |n, n\rangle \langle m, m|, \quad (35)$$

obtained by tracing over the atomic states in the complete density matrix of the tripartite system. The density matrix element $a_{n, m}$, in terms of the coefficients $C_{e, n, n}$ and $C_{g, n, n}$, is $C_{e, n, n} C_{e, m, m}^* + C_{g, n, n} C_{g, m, m}^*$. The von Neumann entropy is

$$S(\hat{\rho}_{F_1, F_2}) = -\text{Tr}[\hat{\rho}_{F_1, F_2} \log_2(\hat{\rho}_{F_1, F_2})], \quad (36)$$

and the quantum relative entropy is

$$E_{F_1, F_2} = -\sum_n a_{n, n} \log_2(a_{n, n}) - S(\hat{\rho}_{F_1, F_2}). \quad (37)$$

The tangles $T_{A, F_1 \otimes F_2}$, $T_{A \otimes F_1, F_2}$ and the relative entropy $E(\hat{\rho}_{F_1, F_2})$ are shown in Figs. 8 and 9 for the system when the initial states are PC and TSV respectively. As in the case of Figs. 6 and 7, the two columns correspond to $k = 0$ and 2×10^{-3} respectively. The three rows of figures correspond to $\Delta = 0$, $\Delta = 0.01 (< \Delta'_c)$, and $\Delta = 0.0161 (= \Delta'_c)$ respectively. The mean photon number of the two modes is taken to be 3. This ensures that the contribution from higher photon number states are negligible and numerical computations are reliable. Firstly, the time evolution profile of the tangle $T_{A \otimes F_1, F_2}$ and the relative entropy E_{F_1, F_2} do not resemble that of the population inversion $W_T(t)$. However, $T_{A, F_1 \otimes F_2}$ which is linear entropy, is related to $W_T(t)$ through

$$W_T^2 = 1 - T_{A, F_1 \otimes F_2} - 4 \left| \sum C_{e, n, n}^* C_{g, n, n} \right|^2. \quad (38)$$

In spite of this relation, the profiles of W_T and $T_{A, F_1 \otimes F_2}$ are not similar. This is in contrast with the single-mode case wherein the profiles of the entanglement resemble with $W_S(t)$, at least for the smaller values of the parameter k . The reason for this dissimilarity is that in the two-mode case, the atomic coherence $|\sum C_{e, n, n}^* C_{g, n, n}|^2$ is comparable to $T_{A, F_1 \otimes F_2}$ and does not become small either for the pair coherent state or the two-mode squeezed vacuum.

The profiles of the tangles and the relative entropy are periodic, when $k = 0$ and $\Delta = 0$, corresponding to the resonant two-mode JC model. When the deformation parameter k is nonzero but small ($= 2 \times 10^{-3}$), the periodicity in the evolution is destroyed. As noted earlier, this feature is present

in the evolution of W_T too. Another interesting aspect is the negative correlation between the time-evolutions of the tangle $T_{A,F_1 \otimes F_2}$ and the relative entropy E , *i.e.*, increase (decrease) of $T_{A,F_1 \otimes F_2}$ is associated with decrease (increase) of E . The negative correlation may be interpreted as redistribution of entanglement, from the field-field entanglement to that between the atom and the two modes. This feature is retained even if k is nonzero implying that the nonlinearity and the intensity-dependent interaction do not hinder the redistribution of entanglement.

In the non-resonant case, the atom does not interact with the field effectively and hence the initial entanglement is not expected to vary much. It is essential to study the cases corresponding to $\Delta = \Delta'_c$ and $\Delta \neq \Delta'_c$. There is an increase of amplitude in the tangle oscillation as k increases to 2×10^{-3} from zero as if the atom-field interaction is effective as in the resonant case. Thus, small non-zero k leads to a “resonance” effect in the non-resonant situation. At slightly larger values of $k \approx 10^{-2}$, the quantity $T_{A,F_1 \otimes F_2}$ becomes insignificant indicating very less entanglement between the atom and the two modes. However, this fact is to be expected; for such values of k the population inversion $W_T(t)$ is nearly unity implying that the atomic state is $\sim |e\rangle$ and hence the atom is not entangled with the fields. The need for larger k , in comparison to $k = 10^{-3}$ in the single-mode case, to disentangle the atom and the two fields is because of the smaller photon number (≈ 3) in the two-mode case.

As in the single mode case, it is useful to define the mean of the tangles and the relative entropy to characterize the effectiveness of the interaction in entangling the systems. Definitions similar to \bar{L} are adopted for the entanglement measures $T_{A,F_1 \otimes F_2}$ and $T_{A \otimes F_1, F_2}$ and the relative entropy E_{F_1, F_2} . The mean is computed over a period T such that $gT = 20$. From the table it seen that there is not as much effect on the mean values with increase of k when compared with the single mode case.

Table 2: Mean tangles and Mean relative entropy in two-mode NJC model

Δ	k	Mean $T_{A,F_1 \otimes F_2}$		Mean $T_{A \otimes F_1, F_2}$		Mean E_{F_1, F_2}	
		PC	TSV	PC	TSV	PC	TSV
0	0	0.39	0.50	1.89	2.41	1.42	1.86
0	2×10^{-3}	0.41	0.7	1.88	2.4	1.38	1.65
0.01	0	0.58	0.58	2.1	2.52	1.45	1.86
0.01	2×10^{-3}	0.61	0.7	1.97	2.51	1.27	1.74
0.0161	0	0.40	0.40	2.08	2.49	1.60	1.98
0.0161	2×10^{-3}	0.66	0.59	2.09	2.51	1.33	1.84

IV. Summary

Nonlinearity and intensity-dependent interactions affect entanglement between an atom and a cavity field. The time-evolution due to \hat{H}_S , wherein

both nonlinearity (Kerr type) and intensity-dependent interaction ($\propto \sqrt{1 + \text{intensity}}$) are included, is exactly solvable. The dynamical symmetry of the Hamiltonian is a deformed Heisenberg-Weyl algebra. When the deformation vanishes, the algebra is the Heisenberg-Weyl algebra. The deformation can be continuously varied so that the algebra is $SU(1,1)$ when the deforming parameter is unity. The deforming parameter has the physical significance that the nonlinearity and the interaction are proportional to it. The Hamiltonians considered in this work approximate many other Hamiltonians that are useful in modeling various quantum optical systems.

The deformed Hamiltonian \hat{H}_S makes the Rabi frequency to attain a minimum value which allows for critical detuning. When the cavity field is chosen so that the mean photon number is \bar{n} and there is critical detuning between the field and the atom, the dynamics exhibits “super structures” in the evolution of population inversion. In the case of single-mode interaction, with a small deformation ($k \approx 10^{-4}$) the evolution of population inversion and entanglement are very different from those in the usual JC interaction ($k = 0$). One of the effects of nonzero k is that the collapses and revivals in the population inversion are less pronounced due to the Kerr nonlinearity. In reality, weak nonlinearities and intensity-dependent interactions are often unavoidable. This implies that in experiments it is really hard to see as many distinct “revivals and collapses” as indicated by the usual single-mode JC model. At resonance, the effect of higher k is to inhibit the evolution of the atom from its excited state. These features are common to both the single-mode and the two-mode NJC models. Some aspects of population inversion dynamics are different for the single-mode and two-mode models. In the undeformed, resonant case the population inversion $W_S(t)$ exhibits ‘collapse-revival’ structure when the initial state is a coherent state and these features are absent if the initial field is a squeezed vacuum. In the two-mode case, such structures are seen when the cavity is either a pair coherent state or a two-mode squeezed vacuum. In the nonresonant case, the deformed Hamiltonian generates more entanglement than the undeformed case. In the resonant case, small deformations tend to reduce the effectiveness of the interaction and hence the entanglement is reduced. In the two-mode case, the tangle $T_{A,F_1 \otimes F_2}$ and the relative entropy E_{F_1, F_2} of the two fields exhibit negative correlation in their dynamics. This is interpreted as the redistribution of entanglement from that between the fields to that between the atom and the fields and vice versa.

Acknowledgment

The authors acknowledge Dr. M. V. Satyanarayana for useful discussions.

References

- [1] E. Schrodinger, *Naturwissenschaften* **23**, 807 (1935).

- [2] E. T. Jaynes and F. W. Cummings, Proc. IEEE **51**, 89 (1963).
- [3] G. Rempe, H. Walther and N. Klein, Phys. Rev. Lett. **58**, 353 (1987).
- [4] B. W. Shore and P. L. Knight, J. Mod. Opt. **40**, 1195 (1993).
- [5] M. Kozierowski and S. M. Chumakov, *Coherence of Photon and Atoms* edited by J. Perina (Wiley, New York, 2001).
- [6] B. Buck and C. V. Sukumar, Phys. Lett. A **81**, 132 (1981).
- [7] W. Vogel and R. L. de Matos Filho, Phys. Rev. A **52**, 4214 (1995).
- [8] R. L. de Matos Filho and W. Vogel, Phys. Rev. A **58**, R1661 (1998).
- [9] P. Gora and C. Jedrzejek, Phys. Rev. A **45**, 6816 (1992).
- [10] A. Joshi and R. R. Puri, Phys. Rev. A **45**, 5056 (1992).
- [11] M. J. Werner and H. Risken, Phys. Rev. A **44**, 4623 (1991).
- [12] S. Sivakumar, J. Phys. A: Math. Gen. **35**, 6755 (2002).
- [13] S. Sivakumar, Int. J. Theor. Phys. **43**, 2405 (2004).
- [14] X. Wang and B. C. Sanders, Phys. Rev. A **65**, 012303 (2001).
- [15] H. Joeng and T. C. Ralph, *Quantum Information With Continuous Variables of Atoms and Light* ed. N. J. Cerf, G. Leuchs and E. S. Polzik (Imperial College Press, 2007).
- [16] S. L. Braunstein and P. van Loock, Rev. Mod. Phys. **77**, 513 (2005).
- [17] P. Tombesi and A. Mocozi, J. Opt. Soc. Am. B **4**, 1700 (1986).
- [18] B. C. Sanders, Phys. Rev. A **45**, 6811 (1992).
- [19] S. J. van Enk, Phys. Rev. Lett. **91**, 017902 (2003).
- [20] S. J. van Enk and O. Hirota, Phys. Rev. A **64**, 022313 (2001).
- [21] G. C. Gerry, J. Optics B **7**, L13 (2005).
- [22] C. L. Chai, Phys. Rev. A **46**, 7187 (1992).
- [23] J. Larson, Journal of Modern Optics **53**, 1867 (2006).
- [24] S. Singh and A. Sinha, Pramana **70**, 887 (2008).
- [25] A. -S. F. Obada, H. A. Hessian and A. -B. A. Mohamed, Opt. Comm. **281**, 5189 (2008).

- [26] C.-Z. Wang, C.-X. Li and G.-C. Guo, Eur. Phys. J. D **37**, 267 (2006).
- [27] X.-P. Liao *et.al*, Physica A **365**, 351 (2006).
- [28] M. Abdel-Aty, M Sebawe Abdalla and A.-S. F. Obada, J. Opt. B: Quantum Semiclass. Opt. **4**, 134 (2002).
- [29] J. H. Eberly, N. B. Narozhny and J. J. Sanchez-Mondragon, Phys. Rev. Lett. **44**, 1323 (1980).
- [30] P. Fillippowicz, J. Phys. A: Math. and Gen. **19**, 3785 (1986).
- [31] X. Hou and B. Hu, Phys. Rev. A **69**, 042110 (2004).
- [32] G. S. Agarwal, J. Opt. Soc. Am. B **5**, 1940 (1988).
- [33] C. M. Caves and B. L. Schumaker, Phys. Rev. A **31**, 3068 (1985).
- [34] P. M. Alsing and G. J. Millburn, Phys. Rev. Lett. **91**, 180404-1 (2003).
- [35] E. Rains, Phys. Rev. A **60**, 179 (1999).

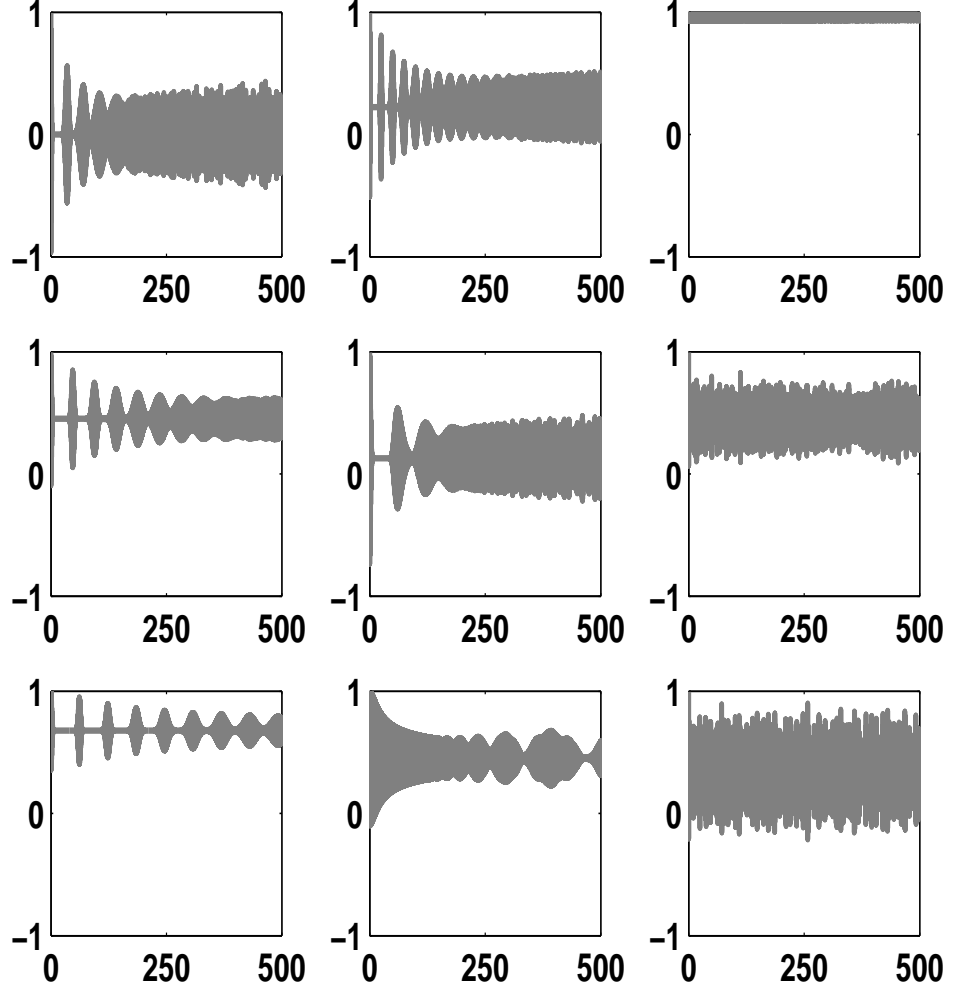


Figure 1: Variation of population inversion versus scaled time (λt) when the initial state is $|\alpha\rangle|e\rangle$; the field state in the coherent state $|\alpha\rangle$ ($\alpha = \sqrt{30}$) and the atom in the excited state $|e\rangle$. The coupling constant is $\lambda = 0.001$. Successive columns correspond to k equal to 0, 10^{-4} , 10^{-3} . In the first and second columns, top most plot corresponds to $\Delta = 0$ and successive plots correspond to $\Delta = 0.01(< \Delta_c)$, $\Delta = 0.016061(= \Delta_c)$. In the third column, top most plot correspond to $\Delta = 0$ and successive plots correspond to $\Delta = 0.05(< \Delta_c)$, $\Delta = 0.061061(= \Delta_c)$.

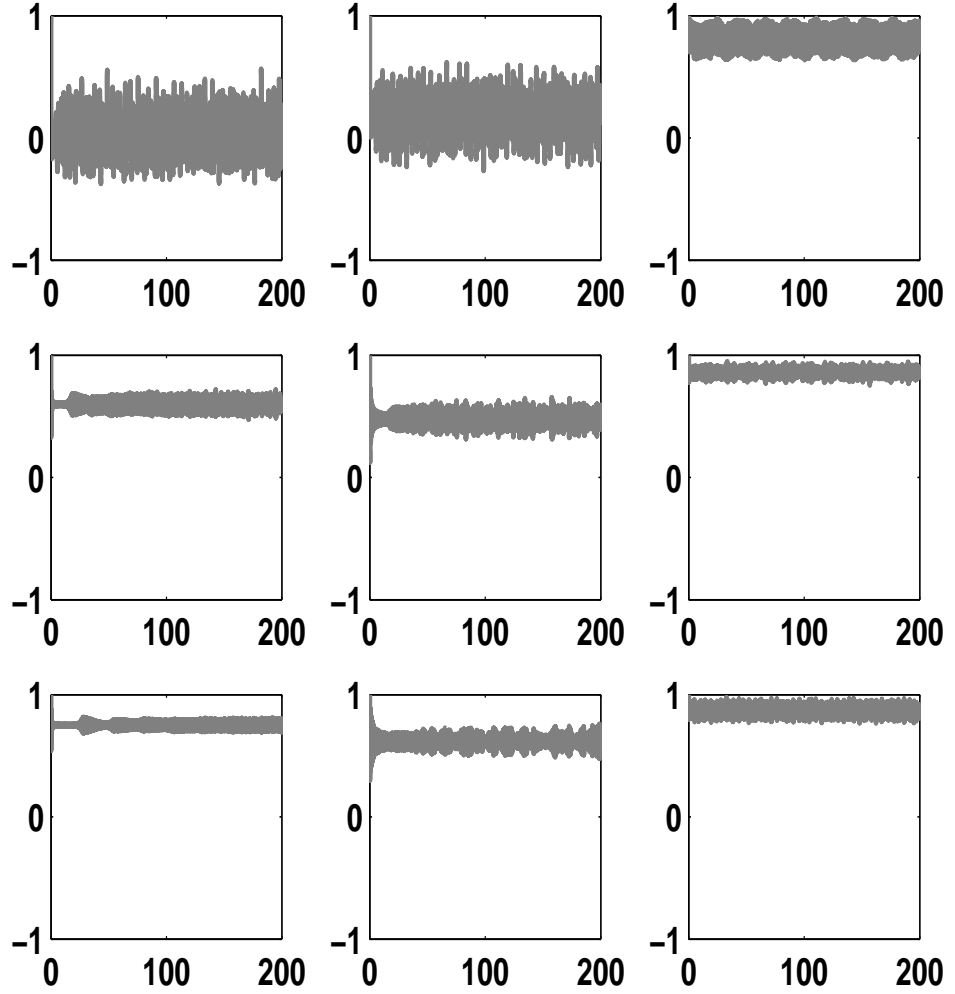


Figure 2: Variation of population inversion with scaled time (λt). The initial state of the field is taken to be squeezed vacuum state $|z\rangle$ ($z = 2.402$) and that of the atom is the excited state $|e\rangle$. Successive columns correspond to k equal to 0, 10^{-4} , 10^{-3} . In the first and second columns, top most plot corresponds to $\Delta = 0$ and successive plots correspond to $\Delta = 0.01(< \Delta_c)$, $\Delta = 0.016061(= \Delta_c)$. In the third column, top most plot corresponds to $\Delta = 0$ and successive plots correspond to $\Delta = 0.05(< \Delta_c)$, $\Delta = 0.061061(= \Delta_c)$. Other parameters are the same as in Fig. 1.

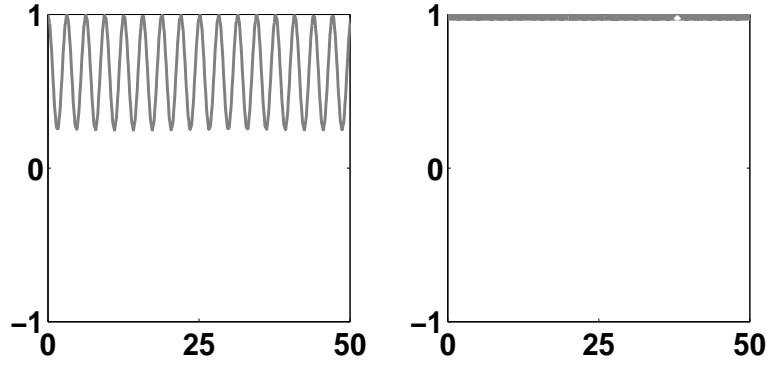


Figure 3: Temporal profile of population inversion with scaled time (λt). The initial state of the field is coherent state $|\alpha\rangle$ and mean number of photons in the mode is $|\alpha|^2 = 1$ (left) and $|\alpha|^2 = 30$ (right). The initial state of the atom is taken to be excited state $|e\rangle$. The interaction is assumed to be resonant ($\Delta = 0$). The coupling constant is $\lambda = 0.001$ and $k = 10^{-2}$.

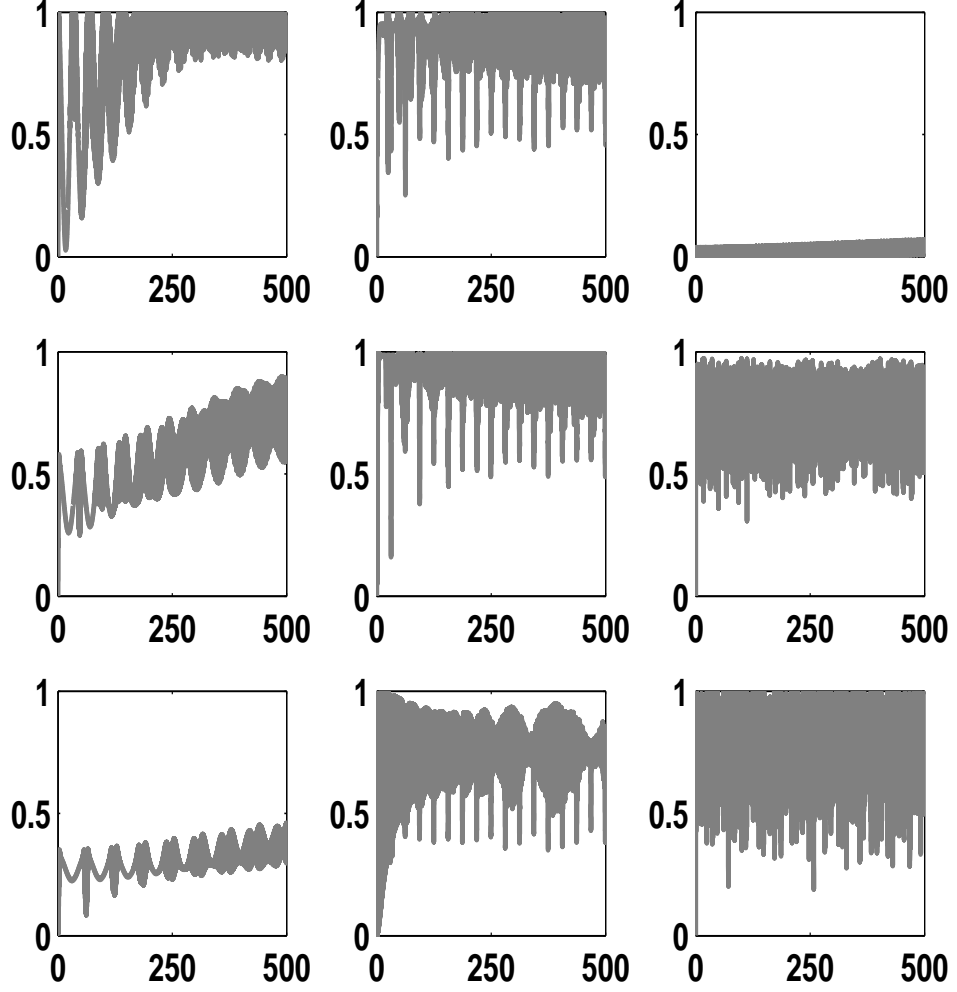


Figure 4: Entanglement versus scaled time (λt). The initial state of the field is the coherent state $|\alpha\rangle$ ($\alpha = \sqrt{30}$) and that of the atom is the excited state $|e\rangle$. Successive columns correspond to k equal to 0, 10^{-4} , 10^{-3} . In the first and second columns, top most plot corresponds to $\Delta = 0$ and successive plots correspond to $\Delta = 0.01(< \Delta_c)$, $\Delta = 0.016061(= \Delta_c)$. In the third column, top most plot corresponds to $\Delta = 0$ and successive plots correspond to $\Delta = 0.05(< \Delta_c)$, $\Delta = 0.061061(= \Delta_c)$. Other parameters are the same as in Fig. 1.

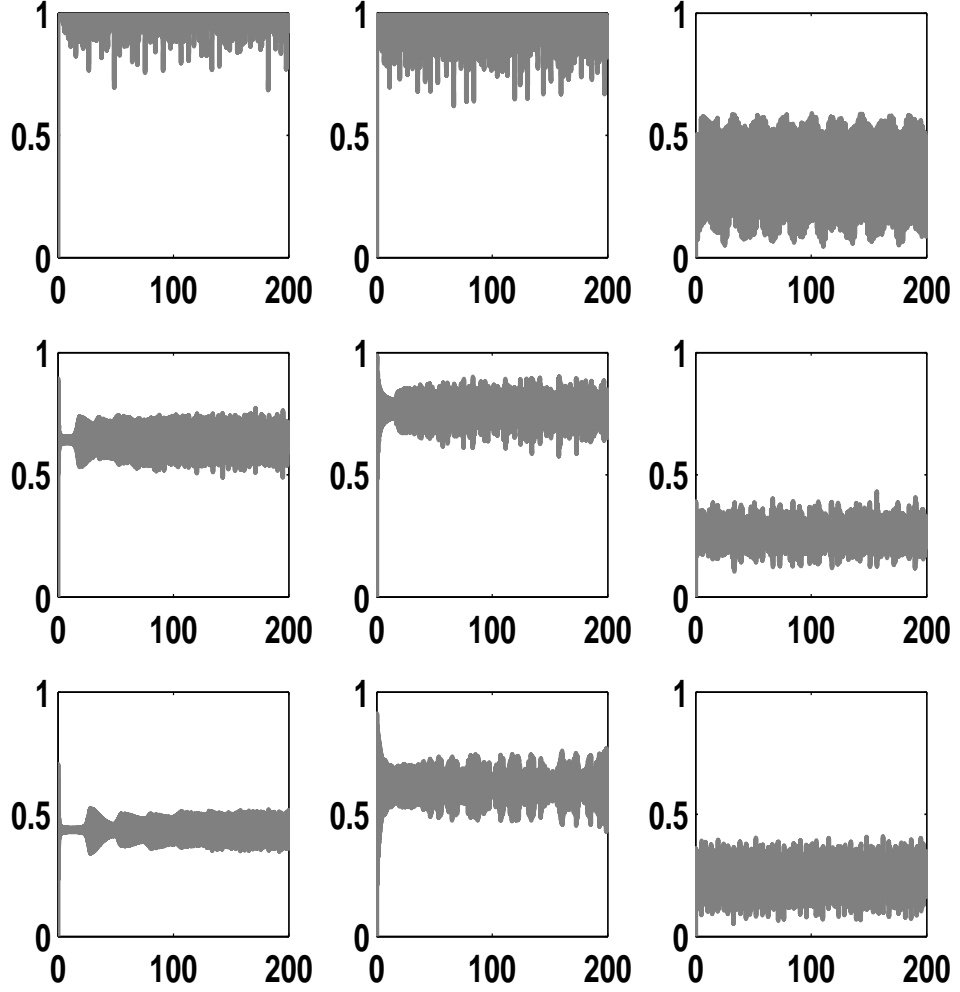


Figure 5: Entanglement versus scaled time (λt). The initial state of the field is the squeezed vacuum state $z\rangle$ ($z = 2.402$) and that of the atom is the excited state $|e\rangle$. Successive columns correspond to k equal to 0, 10^{-4} , 10^{-3} . In the first and second columns, top ost plot corresponds to $\delta = 0$ and successive plots correspond to $\Delta = 0.01(< \Delta_c)$, $\Delta = 0.016061(= \Delta_c)$. In the third column, top most plot corresponds to $\Delta = 0$ and successive plots correspond to $\Delta = 0.05(< \Delta_c)$, $\Delta = 0.061061(= \Delta_c)$. Other parameters are the same as in Fig. 1.

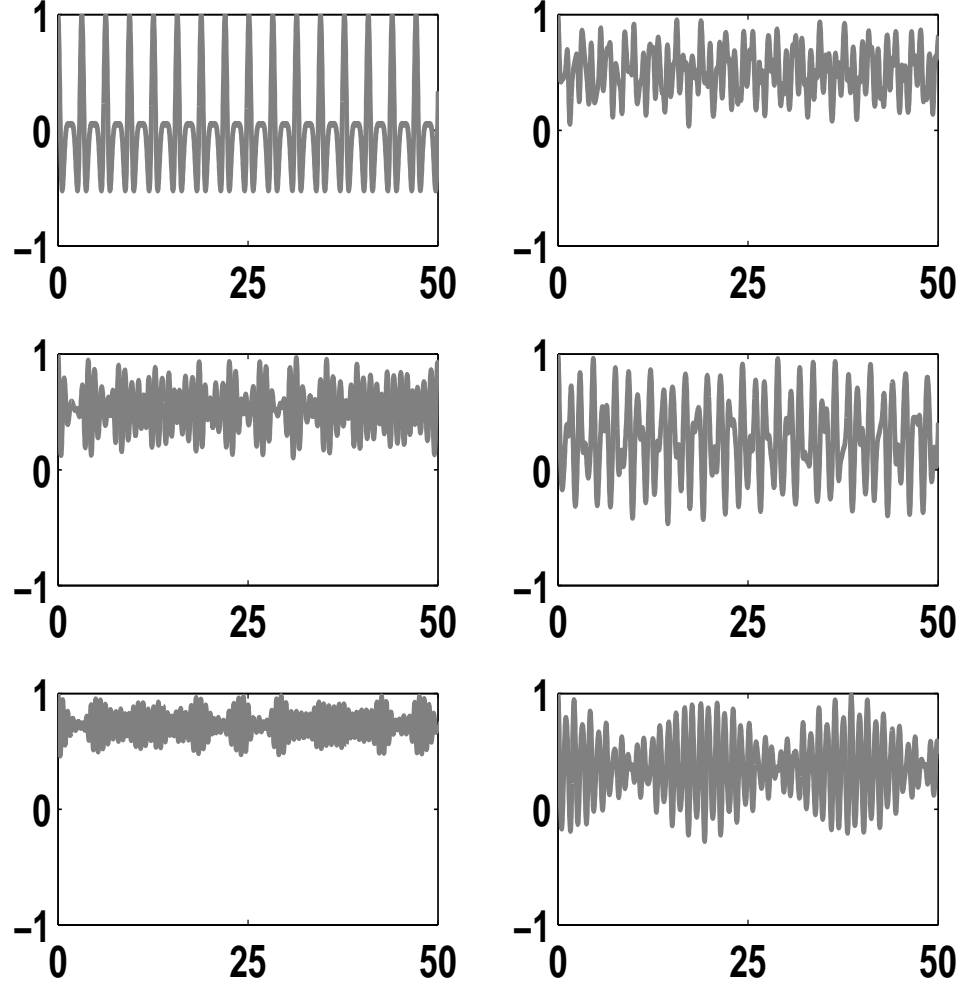


Figure 6: Variation of population inversion with scaled time (λt) when the initial state is $|\zeta\rangle|e\rangle$; the field in the pair coherent state $|\zeta\rangle$ ($\zeta = 1.778$) and the atom in the excited state $|e\rangle$. The coupling constant is $\lambda = 0.002$, the mean number of photons in the field is $\bar{N} = 3$ and the critical detuning is $\Delta'_c = 0.016$. Successive rows correspond to $\Delta = 0$, $\Delta = 0.01 (< \Delta'_c)$, $\Delta = \Delta'_c$. Successive columns correspond to k equal to 0, 2×10^{-3} .

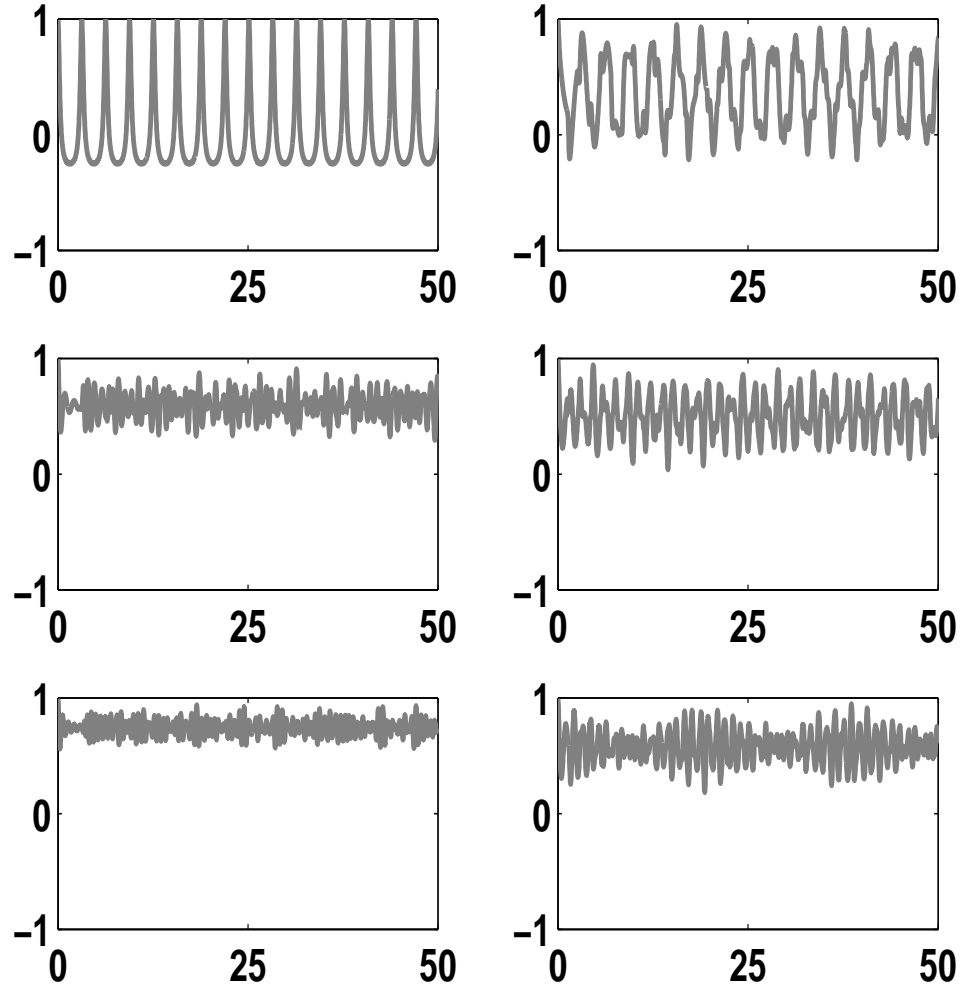


Figure 7: Variation of population inversion with scaled time (λt) when the initial state is $|\mu\rangle|e\rangle$; the field state in the two-mode squeezed vacuum state $|\mu\rangle$ ($\mu = 1.032$) and the atom in the excited state $|e\rangle$. Successive rows correspond to $\Delta = 0$, $\Delta = 0.01(< \Delta'_c)$, $\Delta = \Delta'_c$. Successive columns correspond to k equal to 0, 2×10^{-3} . Other parameters are the same as in Fig. 6.

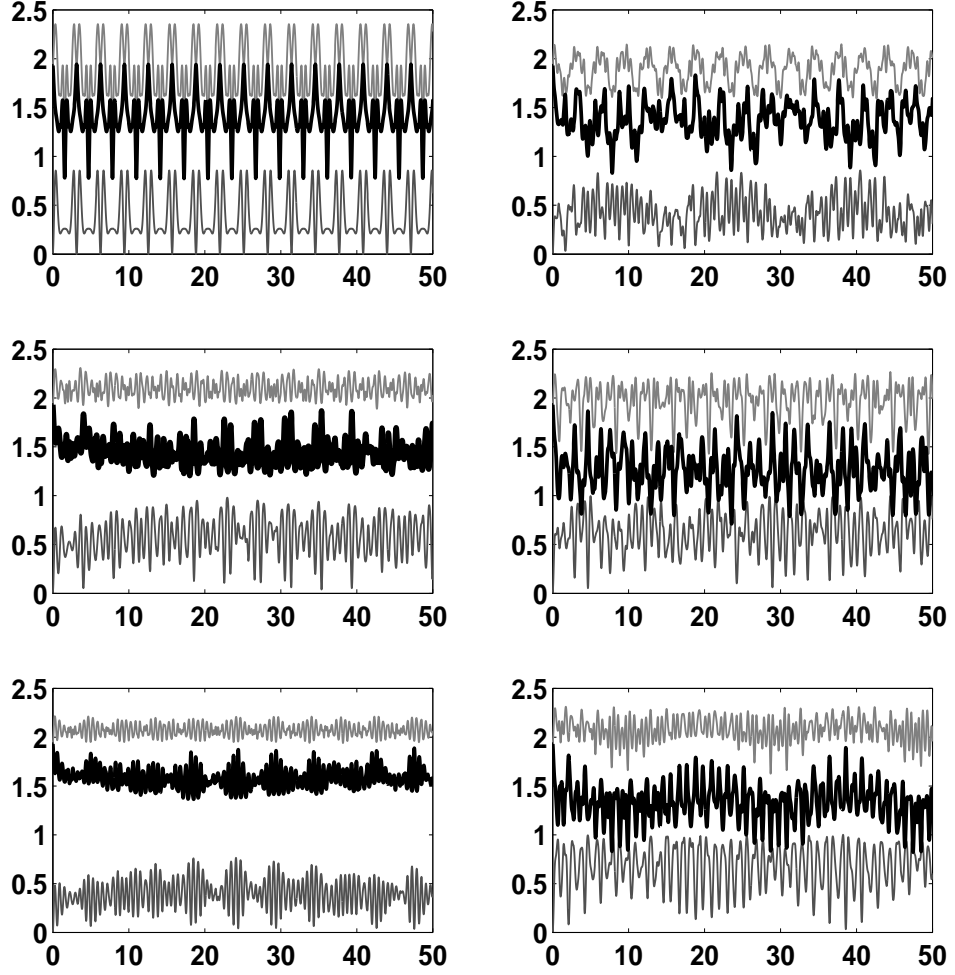


Figure 8: Evolution of various bipartite entanglement measures versus scaled time (λt). The initial state of the field is the pair coherent state $|\zeta\rangle$ ($\zeta = 1.778$) and that of the atom is the excited state $|e\rangle$. The first column corresponds to $k = 0$ and the second column corresponds to $k = 2 \times 10^{-3}$. The top most row corresponds to $\Delta = 0$ and the successive rows correspond to $\Delta = 0.01$ and $\Delta = 0.0161$. In each figures, the quantities shown are $T_{A,F_1 \otimes F_2}$ (bottom), $E(\rho_{F_1, F_2})$ (middle) and $T_{A \otimes F_1, F_2}$ (top). Other parameters are the same as in Fig. 6.

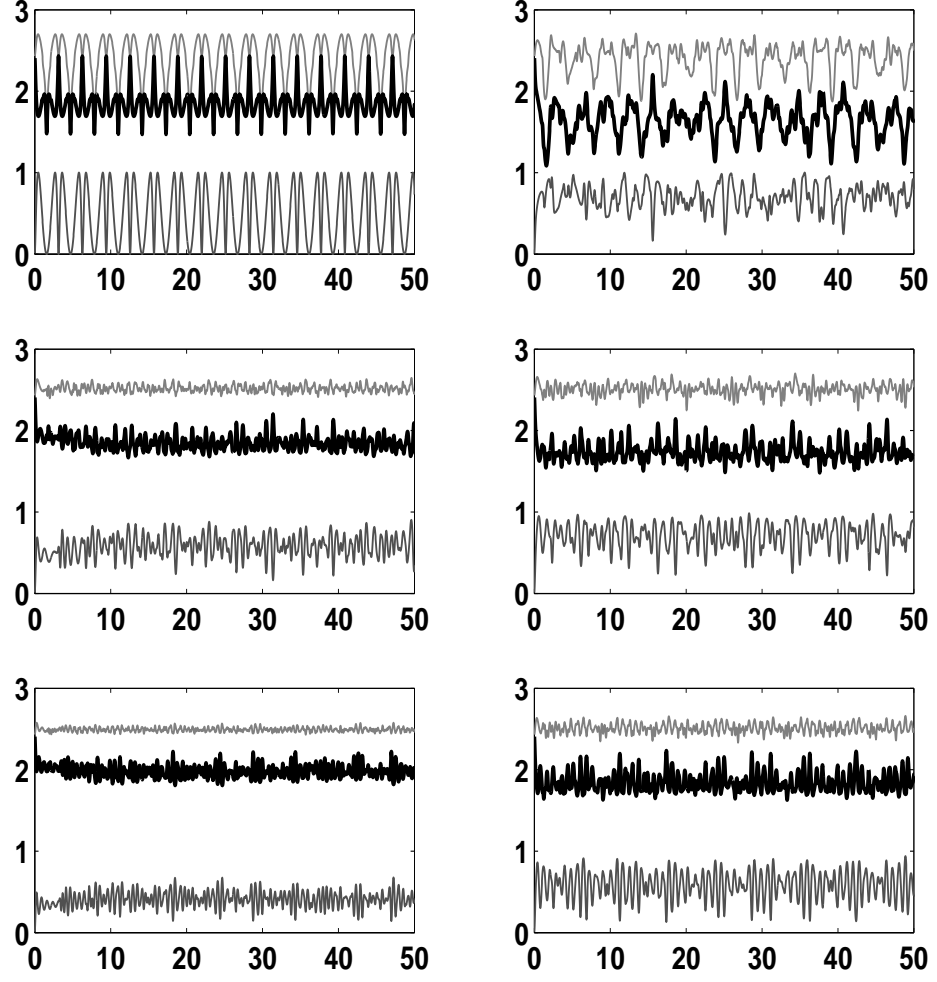


Figure 9: Evolution of various bipartite entanglement measures with time (λt). The initial state of the field is the two-mode squeezed vacuum state $|\mu\rangle$ ($\mu = 1.032$) and that of the atom is the excited state $|e\rangle$. The first column corresponds to $k = 0$ and the second column corresponds to $k = 2 \times 10^{-3}$. The top most row corresponds to $\Delta = 0$ and the successive rows correspond to $\Delta = 0.01$ and $\Delta = 0.0161$. In each figures, the quantities shown are $T_{A,F_1 \otimes F_2}$ (bottom), $E(\rho_{F_1, F_2})$ (middle) and $T_{A \otimes F_1, F_2}$ (top). Other parameters are the same as in Fig. 6.